Iranian Journal of Physics Research, Vol. 25, No. 3, 2025
DOI: 10.47176/ijpr.25.3.12001

Enhancing hydrogen storage capacity using Fe-MWCNT and Co-MWCNT nanoelectrodes

Shokufeh Seifi Elmi[1], Leila Mohammadi[1], Maryam Malmir[1], Faezeh Javanmard[2], Shokufeh Varshoy[3]

1. Department of Physics, Lorestan University, Khorramabad 68151-44316, Iran;
2. Department of Chemistry, Lorestan University, Khorramabad 68151-44316, Iran;
3.University of Technology Sydney

E-mail: malmir.m@lu.ac.ir

(Received 03 November 2024 ; in final form 17 May 2025)

Abstract

In response to the pressing global climate crisis, the quest for sustainable energy alternatives has intensified, with hydrogen emerging as a leading contender due to its clean and renewable nature. This study explores the enhancement of hydrogen storage capacity using novel nanoelectrodes, specifically Cu-Fe-MWCNT and Cu-Co-MWCNT, as negative electrodes. The synthesis of these nanoelectrodes was achieved through an electrodeposition process, and their structural and compositional properties were examined using X-ray diffraction (XRD), Energy-dispersive X-ray spectrum (EDX), and scanning electron microscopy (SEM). The hydrogen storage capabilities of these materials were assessed via chronopotentiometry. The findings reveal that the Fe/MWCNT nanocomposite electrode offers improved stability and efficiency in hydrogen storage compared to the Co/MWCNT electrode, suggesting its potential as a superior material for electrochemical hydrogen storage applications. This research contributes to the advancement of hydrogen storage technologies and supports the role of hydrogen in the sustainable energy ecosystem.

Keywords: Co/MWCNT and Fe/MWCNT nanoelectrodes , Nanostructures, Electrochemical, Hydrogen storage

1. Introduction

Nowadays, all researcher people are fighting for survival and the planet's future. It is a war against climate change. It has dramatic consequences for the future of our lives that can kill thousands. The primary root cause of it is over-dependence on fossil fuels such as coal and natural gas. Hydrogen can massively enhance the energy security of countries all over the world. It is becoming a potential substance for a new energy future to meet the climate crisis challenge to establish energy independence from fossil fuels because of these reasons: 1. renewable energy and high availability; hydrogen can be produced using various renewable energy sources such as water electrolysis [1] and ammonia electrooxidation [2] where electricity splits water molecules into hydrogen and oxygen; 2. zero emissions; hydrogen fuel cells generate electricity by combining hydrogen and oxygen, and the reaction that occurs does not produce any air pollutants or greenhouse gases. On the other hand, the only by-product is water vapor [3], making it a clean energy carrier. 3. energy density; hydrogen has a high energy density [4], meaning it contains a large amount of energy per unit of weight. This makes it an efficient energy carrier, especially for applications that require long-range or high-energy density, such as transportation. Hydrogen fuel cells can power electric vehicles [5], providing an alternative to fossil fuel-powered cars and reducing dependence on oil. 4. Versatile Applications: Hydrogen can be used in various sectors, including transportation, industry, and power generation [6, 7]. Nonetheless, ongoing research and development efforts are focused on addressing these challenges and unlocking the full potential of hydrogen as a vital component of a sustainable energy future. Much research has been conducted on improving hydrogen storage capacity using nanostructured materials like nanoparticles [8], nanotubes [9], nanofibers [10], and nanoelectrodes [11]. CNTs possess many unique properties, like a vast high surface, a very low volumetric density, low mass density, high porosity, and chemical stability [12]. In addition, there is a way to increase capacity by the adsorption sites of CNTs, which means acid treatment. The acid treatment causes modification and purification CNTs to create further adsorption sites by cutting and creating faults [4, 13-16].

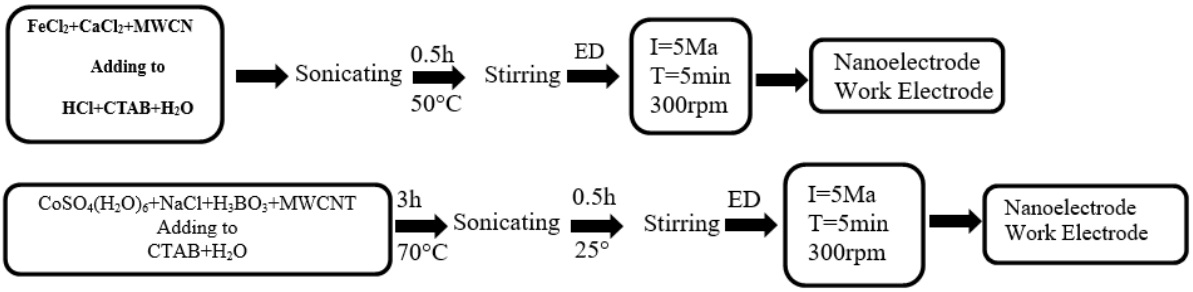

Figure. 1. Schematic flow chart of bath composition and electrodeposition condition.

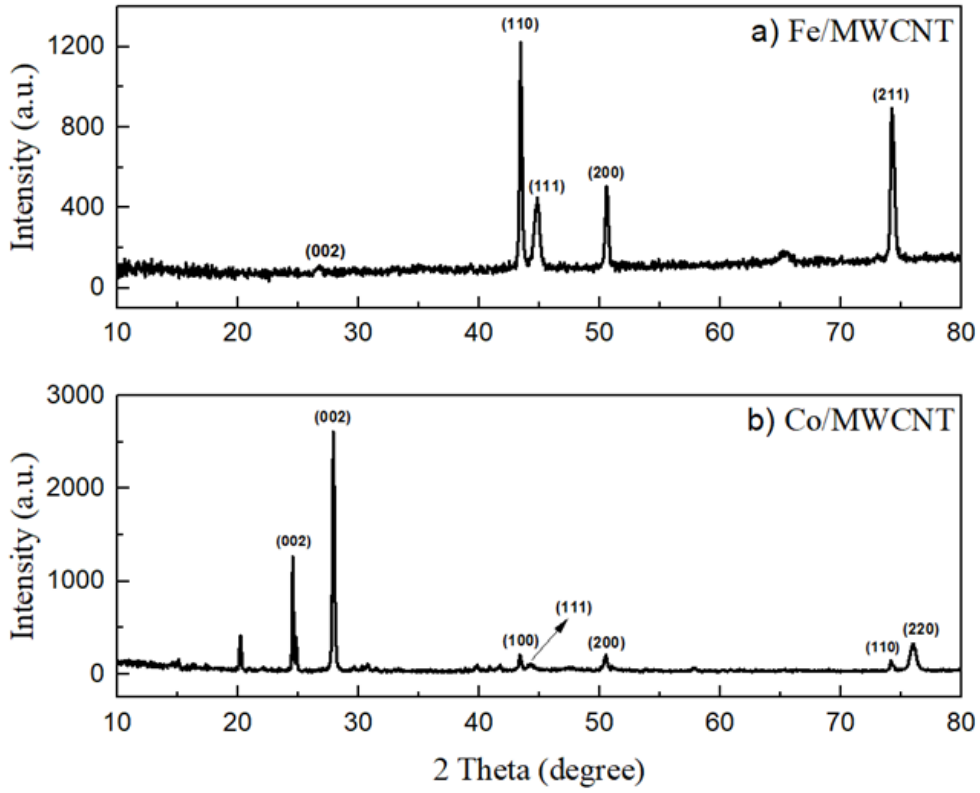

Figure. 2. XRD diffractograms of (a) **Co/MWCNT** and (b) **Fe/MWCNT** nanoelectrodes.

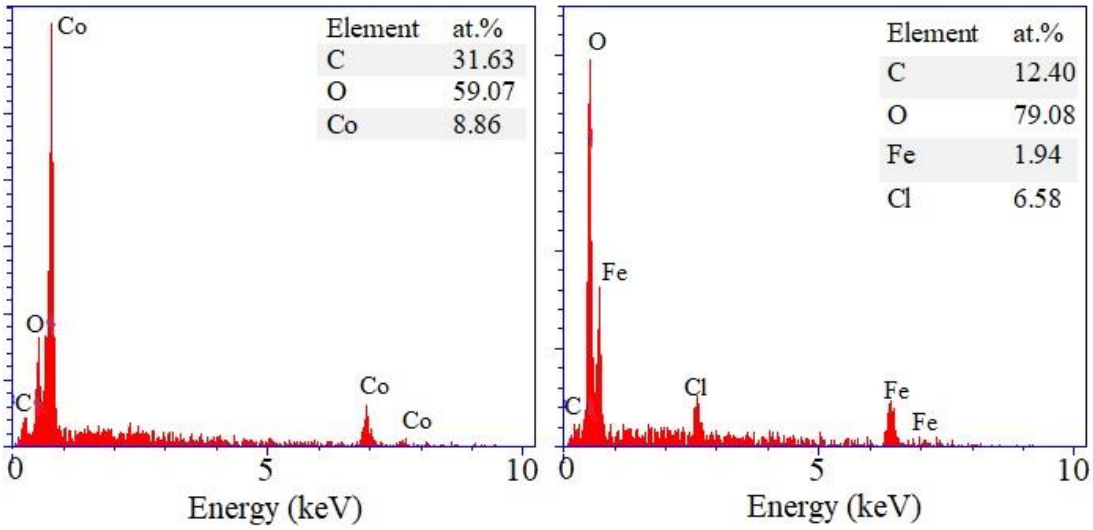

Figure. 3. The EDX spectrum of (a) **Co/MWCNT** and (b) **Fe/MWCNT** nanoelectrodes.

On the other hand, the attraction sites of CNT can be enhanced by adding different transition metals like Ni [17], Pt [18], Pd [19], Cu [20], Co [21], Fe [21], Ag [22] and Sn [4] due to an increase in the binding of H atoms onto metal-CNT and sometimes act as a catalyst (Bordbar article) [22], It is worth noting that the manufacturing method of these electrodes is different from the manufacturing method of the nanoelectrodes in this study, and the manufacturing method can be a factor affecting the hydrogen storage capacity. In other words, more dopants can increase carbon nanotubes' binding strength and uptake capacity because transition metals transfer electrons to carbon atoms [21]. Among these metals, Fe and Co are two elements that choose to combine with CNTs for this study. Hence, in the present research, Fe-MWCNT and Co-MWCNT nanoelectrodes are fabricated as new negative electrodes for hydrogen storage. This work investigated and compared the effects of Fe and Co on CNTs for the electrochemical hydrogen storage capacities. Here, we used the electrodeposition method for depositing nanoelectrodes (as a combination of Co (Fe) with MWCNTs) on copper substrate and then used XRD, FT-IR and SEM to evaluate their structures.

2. Experimental

2.1. Materials and Characterization

The precursors used in the synthesis of the Fe-MWCNT and Co-MWCNT nanoelectrodes included iron (II) chloride ($FeCl_2$), calcium chloride (CaCl2), cobalt (II) sulfate hexahydrate ($CoSO_4 \cdot 6H_2O$), sodium chloride (NaCl), boric acid (H_3BO_3), cetyltrimethylammonium bromide (CTAB), and hydrochloric acid (HCl). These were purchased from Merck and used without further purification. Multi-walled carbon nanotubes (MWCNTs) were obtained from US Research Nanomaterials, Inc., with a purity greater than 95%, outside diameters of 20–30 nm, and an electrical conductivity exceeding 100 S/cm. Scanning electron microscopy (SEM) images were acquired using a MIRA3 TESCAN field emission scanning electron microscope equipped with an Energy-Dispersive X-ray (EDX) analyzer. X-ray diffraction (XRD) patterns were obtained using an X'PertPro diffractometer with monochromatized Cu Kα radiation (λ = 1.54 Å). The hydrogen storage capacity of the nanoelectrodes was assessed using the chronopotentiometry method with a three-electrode setup consisting of a platinum (Pt) counter electrode, a silver/silver chloride (Ag/AgCl) reference electrode, and the synthesized nanocomposite as the working electrode. Measurements were conducted in a 6M KOH electrolyte solution to determine the charge and discharge capacities. These analyses were performed using a SAMA 500 electrochemical device.

2.2. Fabrication of Fe (Co)-MWCNT Nanoelectrode

The Fe-MWCNT nanoelectrode was synthesized via an electrodeposition method, as illustrated in figure 1. The procedure was: $FeCl_2$, $CaCl_2$, and MWCNT were added to a solution containing HCl, CTAB, and deionized water. The mixture was then sonicated at 50°C for 3 hours, followed by magnetic stirring at 50°C for 30 minutes. Finally, by electrodeposition method, a homogeneous layer of Fe-MWCNT was deposited onto a copper substrate by applying a current of 5 mA for 5 minutes, with continuous stirring at 300 rpm to ensure uniformity. The same procedure was employed to synthesize the Co-MWCNT nanoelectrode. The chemical solution comprised $CoSO_4$.6 (H2O), NaCl, H_3BO_3, and MWCNT were added to a solution containing CTAB, and deionized water. This mixture underwent ultrasonication for 3 hours at 70°C, followed by magnetic stirring for 0.5 hours at 25°C. Ultimately, a layer of Co-MWCNT was deposited onto the copper substrate using a current of 5 mA for 5 minutes with continuous stirring at 300 rpm to ensure uniformity.

3. Results and Discussion

The XRD patterns of Fe/MWCNT and Co/MWCNT nanocomposites reveal distinct crystalline features associated with both the metal phases and the carbon nanotube framework. In both spectra, a broad diffraction peak centered at approximately $2\theta \approx 27°$ corresponds to the (002) plane of graphitic carbon, confirming the presence of multi-walled carbon nanotubes (MWCNTs) with graphitized structure. In some samples, a peak is observed around $2\theta \approx 20°$, which may indicate the presence of disordered carbon phases, amorphous carbon impurities, or turbostratic stacking due to random alignment and structural defects in the nanotubes. This shift and broadening can also be attributed to nanoscale size effects and the interactions between MWCNTs and metal nanoparticles. In the Fe/MWCNT composite (Figure 2a), characteristic reflections at approximately $2\theta \approx 43.5°$, 44.8°, 50.5°, and 74.2° are attributed to the (110), (111), (200), and (211) planes of bcc α-Fe (JCPDS No. 06-0696), confirming the formation of crystalline iron nanoparticles. Additionally, weak but identifiable peaks between 60° and 70° further support the presence of a cubic iron phase. For the Co/MWCNT sample (Figure 2b), major peaks appear at $2\theta \approx 44.2°$, 50.5°, and 75.9°, matching the (111), (200), and (220) planes of fcc cobalt (JCPDS No. 15-0806). Notably, a minor peak around $2\theta \approx 74°$ corresponds to the (110) plane of hexagonal close-packed (hcp) Co, indexed with JCPDS No. 00-008-0415, indicating a possible secondary hcp cobalt phase with low relative abundance. Furthermore, a set of weak reflections in the $2\theta \approx 18–33°$ range is attributed to monoclinic cobalt oxalate phases (C_2O_4Co), suggesting partial oxidation or precursor residue. Overall, the observed diffraction patterns confirm the successful synthesis of metal-loaded MWCNT composites with distinct crystalline metal phases and carbon structures. The position, intensity, and width of the carbon-related peaks provide insight into the degree of graphitization, crystallite size, and the influence of metal incorporation on the nanotube structure.

The energy-dispersive X-ray spectrum (EDX) is utilized to further confirm and evaluate the purity of the synthesized samples (Co/MWCNT and Fe/MWCNT nanoelectrodes), as shown in figure 3. It is evident that the chemical composition of the Co/MWCNT electrode consists of the elements Co, O, and C, with atomic percentages of 8.86%, 59.07%, and 31.63%, respectively.

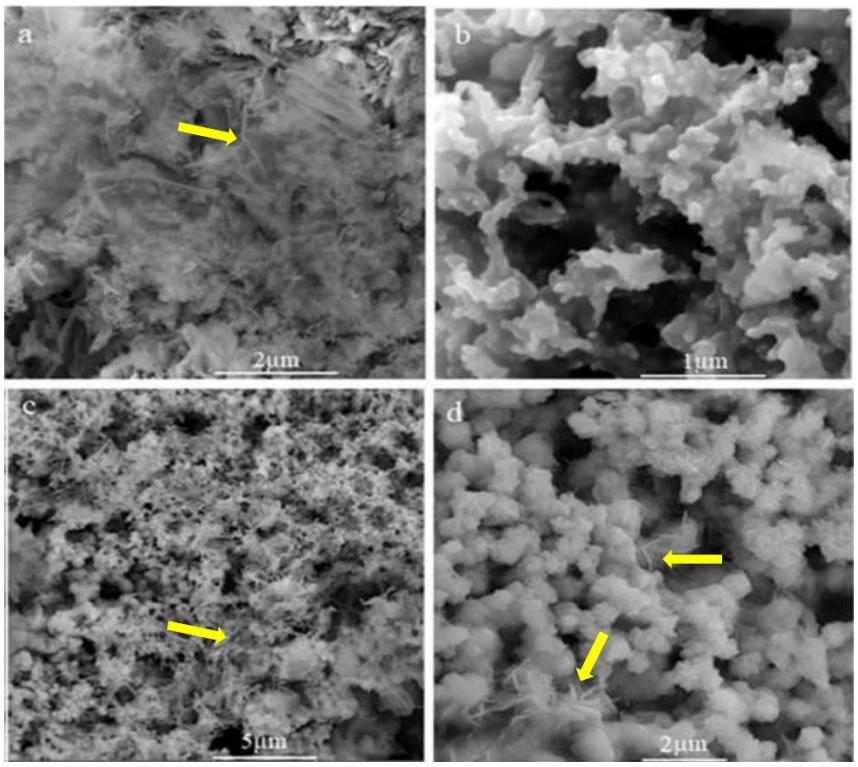

Figure. 4. SEM photograph of (a, b) **Co/MWCNT** and (c, d) **Fe/MWCNT** nanoelectrodes.

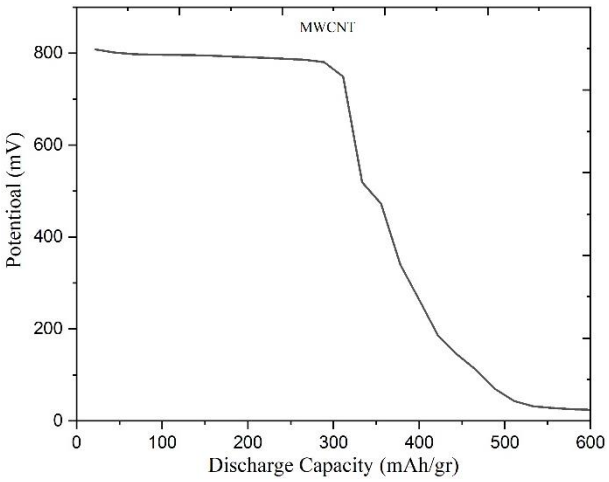

Figure. 5. The first cycle discharge capacity of MWCNTS.

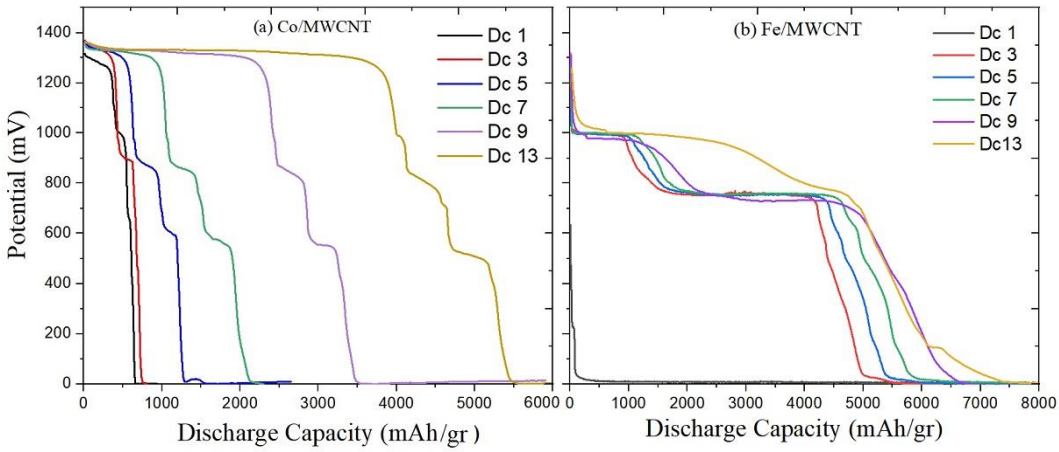

Figure. 6. Thirteen cycles discharge capacity profiles of (b) **Co/MWCNT** and (c) **Fe/MWCNT** nanocomposite in current

Similarly, the Fe/MWCNT electrode is composed of the elements Fe, O, C, and Cl, with atomic percentages of 1.94%, 79.08%, 12.40%, and 6.58%, respectively. This analysis underscores the high purity and precise composition of the synthesized nanoelectrodes.

The scanning electron microscope (SEM) images presented in figure 4 illustrate the microstructural characteristics of two distinct carbon nanotube-based materials. figures (a) and (b) depict the morphology of Co-multi-walled carbon nanotubes. These nanotubes exhibit a highly interconnected and entangled three-dimensional network-like structure, with individual nanotubes displaying a curved and wavy appearance. This unique microstructural feature is likely attributed to the incorporation of cobalt within the carbon nanotube framework. In contrast, figures (c) and (d) showcase the microstructure of iron-multi-walled carbon nanotubes (Fe-MWCNTs). In this case, the nanotubes appear more fragmented and less interconnected compared to the Co-MWCNTs. Furthermore, the individual Fe-MWCNTs exhibit a relatively rougher surface texture, suggesting the presence of iron within the nanotube structure. This morphological difference could be advantageous for applications where controlled porosity and accessibility of the nanotubes are essential, such as catalysis or energy storage. The rougher surface texture of the Fe-MWCNTs may also provide increased opportunities for surface functionalization or the anchoring of active species.

Electrochemical hydrogen storage

The discharge behavior of the nanoelectrodes synthesized on a copper foam substrate was systematically investigated in a 6 M KOH aqueous solution at a current density of 1mA and room temperature. Figure 5 showes The first cycle discharge capacity of MWCNTS. As illustrated in figure 6, the Co/MWCNT nanoelectrode exhibits a notable increase in discharge capacity with cycling, reaching approximately 5000 mAh/g by the 13th cycle. This enhancement in discharge capacity can be attributed to a gradual activation process that increases the availability of electrochemically active sites, thereby improving hydrogen storage efficiency. In contrast, the Fe/MWCNT nanocomposite maintains a significantly higher and more stable discharge capacity of approximately 7500 mAh/g during the same cycle. Both of nanoelectrodes Fe (Co)-MWCNTs showe more discharge capacity than alone MWCNTs one, even in the first sycle. This superior performance is indicative of the enhanced structural stability and superior electron transfer properties of the Fe-based electrode, which facilitate more effective hydrogen absorption and desorption processes. The structural integrity of Fe/MWCNT is preserved better than that of Co/MWCNT throughout cycling, contributing to its consistent performance and reduced capacity fading. These findings underscore the potential of Fe/MWCNT as a more effective material for applications requiring reliable and long-term hydrogen storage, highlighting its advantages in both capacity and cycling stability compared to Co/MWCNT.

4. Conclusion

In this study, we have successfully synthesized and characterized Fe-MWCNT and Co-MWCNT nanoelectrodes for their application as negative electrodes in electrochemical hydrogen storage systems. The data reveal that the Fe/MWCNT nanocomposite demonstrates significantly higher discharge capacity, achieving around 7500 mAh/g, in contrast to the Co/MWCNT's peak discharge capacity of approximately 5000 mAh/g after 13 cycles. This superior performance is likely attributed to the Fe/MWCNT electrode's more stable crystal structure and enhanced ability to transfer electrons within an alkaline environment. These results highlight the promising potential of the Fe/MWCNT nanocomposite as a material for electrochemical hydrogen storage, providing a pathway for efficient and stable storage solutions. Furthermore, this work not only advances the field of hydrogen storage technology but also underscores the significance of ongoing research and development in materials science to address the challenges associated with the widespread adoption of hydrogen as a sustainable energy source. Future research will aim to further optimize the structure and composition of these nanoelectrodes to enhance their hydrogen storage capacity and cycling stability. Additionally, there will be a focus on integrating these nanoelectrodes into functional hydrogen storage systems, with the ultimate goal of transitioning them to commercial use in the energy industry and supporting the global shift towards cleaner and more sustainable energy practices.

References

1. J Chi and H Yu, *Chinese J. Catal.* **39** (2018) 390.
2. N M Adli, H Zhang, S Mukherjee, and G Wu, *J. Electrochem. Soc.* **165** (2018) J3130.
3. Sh Varshoy, B Khoshnevisan, M Mohammadi, and M Behpour, *Physica B* **526** (2017) 143.
4. S Varshoy, B Khoshnevisan, and M Behpour, *Int. J. Hydrogen Energy* **44** (2019) 6674.
5. B Tanç, H T Arat, E Baltacıoğlu, and K Aydın, *Int. J. Hydrogen Energy* **44** (2019) 10120.
6. P Nikolaidis and A Poullikkas, *Renew. Sustain. Energy Rev.* **67**(2017) 597.
7. H B Navaid, H Emadi, and M Watson, *Int. J. Hydrogen Energy* **48** (2023)10603.
8. A Zonarsaghar, M M Kamazani, and S Z Ajabshir, *J. Mater. Sci. Mater. Electron.* **33** (2022) 6549.
9. K Kajiwara, H Sugime, S Noda, and N Hanada, *J. Alloys Compd.* **893**, 162206 (2022).
10. L Ren, W Zhu, Q Zhang, C Lu, F Sun, X Lin, and J Zou, *Chem. Eng. J.* **434** (2022) 134701.
11. S Varshoy, B Khoshnevisan, and M Behpour, *Nanotechnology* **29** (2018) 075402.
12. S U Rather, *Int. J. Hydrogen Energy* **45** (2020) 4653.
13. S U Rather, R Zacharia, M Naik, S W Hwang, A R Kim, and K S Nahm, *Int. J. Hydrogen Energy* **33** (2008) 6710.

14. R Strobel, J Garche, P T Moseley, L Jorissen, and G Wolf, *J. Power Sources* **159** (2006) 781.
15. Y Ren and D L Price, *Appl. Phys. Lett.* **79** (2001) 3684.
16. S Patchkovskii, J S Tse, S N Yurchenko, L Zhechkhov, T Heine, and G Seifert, *Proc. Natl. Acad. Sci.* **102** (2005) 10439.
17. M Mohammadi, B Khoshnevisan, and S Varshoy, *Int. J. Hydrogen Energy* **41** (2016) 10311.
18. S J Yang, J H Cho, K S Nahm, and C R Park, *Int. J. Hydrogen Energy* **35** (2010) 13062.
19. S C Mu, H L Tang, S H Qian, M Pan, and R Z Yuan, *Carbon* **44** (2006) 762.
20. S Li, W Pan, and Z Mao, *Int. J. Hydrogen Energy* **30** (2005) 643.
21. A Reyhani, S Z Mortazavi, S Mirershadi, A Z Moshfegh, P Parvin, and A Nozad Golikand, *J. Phys. Chem. C* **115** (2011) 6994.
22. M Bordbar, T Alimohammadi, B Khoshnevisan, B Khodadadi, and A Y Faal, *Int. J. Hydrogen Energy* **40** (2015) 9613.